Creating a beam propagation framework using an extended Crank-Nicolson algorithm

Andrei-Horatiu Eftime – Merton College, University of Oxford

Abstract

We analyze several methods of implementing computational frameworks for laser beams propagating through plasma channels. The algorithms discussed are the modal reconstruction, the beam propagation method (BPM), the Crank-Nicolson algorithm, and a method based on the Uniaxial Pulse Propagation Equation (UPPE). We will split them in two categories, based on the underlying technique of each: Fourier methods (UPPE, BPM and modal reconstruction) and finite difference methods (Crank-Nicolson algorithm). We compare the physical reliability, complexity, and limitations of Fourier methods and finite difference methods. Furthermore, we showcase how the finite difference algorithm works on some well-known physical situations.

Introduction

Computer simulations are a crucial part of laser physics, helping researchers find setups that are worth investigating experimentally. Furthermore, they can substitute experiments in some situations. Therefore, there are several algorithms that can be used to propagate a beam through a channel, at least 4 different methods described in [3] and another 2 described in [1]. One reason for the existence of multiple methods is that there is no method that exactly describes the propagation within a reasonable complexity. Although the methods are applicable to any form of signals, we will only demonstrate how they work on Gaussian signals.

Each method corresponds to a set of approximations applied to the Maxwell equations, therefore, based on the situation, some approximations might be more suitable than others. We distinguish two classes of methods: those which solve the propagation in the frequency domain, the Fourier methods, and those which solve it in the real space using the infinitesimal changes in the electric field, the finite difference methods. We make this separation although some of the Fourier methods make use of finite difference methods in the process.

Physical accuracy is the primary criterion by which we are going to judge the methods. In addition, we want to be able to propagate the pulse through a physically relevant distance in a reasonable time. Physically relevant distances for a laser pulse are usually expressed as multiples of the Rayleigh range ($z_R = \frac{\pi w_0^2}{\lambda}$, where w_0 is the width of the beam and λ is the wavelength of the beam) therefore, from now on, we will denote the complexity of our algorithms with $O\big(f(n)\big)$, where n is the number of Rayleigh ranges over which we propagate and $f(n)$ is the functional on which it depends. Besides the complexity, the corresponding constant in each method will also be reviewed, as, in some cases, it might be considerably large. We will analyze the prerequisites for each of the algorithms, what information about the channel is needed, and how feasible it is to obtain this information. Lastly, we analyze their limitations, and suggest in which regimes or circumstances each method is recommended. All the limitations will be set empirically, based on the point where we can see a deviation from the expected shape or dependence of the result.

Fourier Methods

Laser pulses comprise a range, or a discrete combination, of frequencies. Also, recurring equations, such as the Helmholtz equation and the paraxial wave equation ([1.25], [1.41] from [4]) are easier to solve in the frequency domain. In general, Fourier methods allow for propagations with larger steps than the finite difference methods. Consequently, Fourier methods are popular in solving propagation equations. One common issue with this class of methods is that, given that our grid is finite, the Fourier transform brings unwanted, unphysical reflections at the boundaries. In what follows, we will analyze

three methods based on Fourier transforms.

Beam Propagation Method

This method is described in section 2.4 of [1]. The starting code on which the simulation is based is [5]. The advantages of this method are the low number of known parameters needed (the wavelength of the laser and the plasma profile), the low complexity and the accurate depiction of non-leaky channels. The disadvantages of this method are the aforementioned reflections and the representation of leaky channels.

In the transverse direction, we need a resolution comparable to the wavelength of our pulse (around 1000 nm), and we also need a region of interest larger than the width of the beam (the radial distance over which the intensity of the beam decreases by a factor of e) at any point. The graphs in Figure 1 were obtained with a 512x512 grid, however, we can obtain sensible results even with a 200x200 grid. The advantage of this method is that the step size can be as large as a third of a Rayleigh range at a time. At each step, we go through the whole grid a couple of times. Considering these aspects, the complexity of this algorithm in a non-leaky regime is $O(n)$ with a constant of $200\,x\,200\,x\,50 = 2x10^6$.

As we notice in Figure 1 (a) and (b), despite a few dim reflections, we have a faithful representation of the HOFI channel. In Figure 1 (d) we observe a free space propagation. While the defocusing is well represented, lost energy reappears due to the Fourier reflections, which results in the unphysical situation represented in Figure 1 (c). A solution to this issue would be enlarging the grid in both directions proportionally to the increase in the propagation distance. This would result in a complexity $O(n^3)$ if the dispersion is linear in z, or $O(n^5)$ if the dispersion is parabolic.

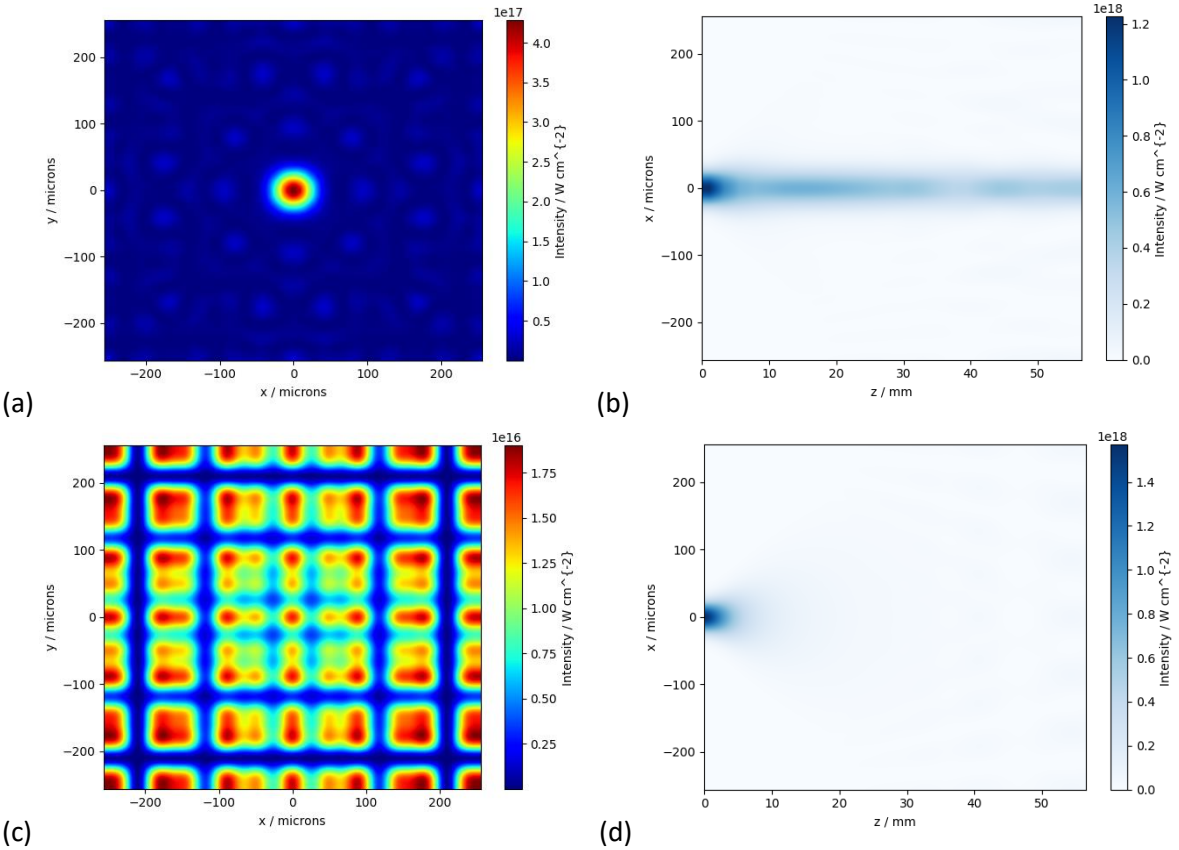

Figure 1: Propagation of a Gaussian beam of wavelength $\lambda_0 = 800\text{nm}$, initial spot size $w_0 = 100\mu m$ um over a distance of 16 $z_R$with (a,b) and without (c,d) a HOFI plasma channel of matched spot size $w_0 = w_m$, as calculated by a BPM code. (a, c): the transverse intensity profiles of the beam in the exit

plane of the channel. (b, d) the longitudinal variation of the beam intensity in the plane y = 0. For these simulations a 512 x 512 transverse grid was employed, and 250 longitudinal steps were used.

Modal Reconstruction

This method is based on equation [76] from [3], it aims to compute the field at each step through direct integration of the contributions of each mode of the channel. In this approach, we assume the current J to be zero, and we assume that the polarization oscillates harmonically, therefore we substitute the time derivative with the frequency ω in equation [76] from [3]. For the modes, the results from equation [4.7] of [2] were considered.

We abandoned after obtaining drastically unphysical results with these approximations.

UPPE

This approach is based on the Uniaxial Pulse Propagation equation (equation [93] of [3]):

$$\frac{\partial E_{k_x,k_y}(\omega,z)}{\partial z} = \mathrm{i}K_z E_{k_x,k_y} + \mathrm{i}\frac{\omega^2 P(\omega,z)}{2\epsilon_0 c^2 K_z(k_x,k_y,\omega)} \qquad (1)$$

In order to solve this, we tried using finite difference methods, incrementing the field on the right-hand side times a small dz, which has to obey $K_z dz \ll 1$ to retain the numerical stability of the solution. However, this significantly reduces the distance over which we can propagate the signal. Comparing this approach with the beam propagation method, the transverse constant is the same because we need to compute a Fourier transform at each step, however, the longitudinal constant would increase by a factor of 10^3. Given that this approach also retains the reflection issues due to the use of Fast Fourier Transforms, while being a thousand times slower, it was concluded that, for all practical purposes, this approach was worse than the beam propagation method. Therefore, this method was abandoned.

Finite Difference methods

The pure finite difference methods have the advantage of being free from the unphysical reflections caused by Fourier transforms. However, depending on the method used, the stability of the solution can require restrictive conditions on the step size used for the iteration, and, consequently, can cause an increase in the execution times. There are some methods, called implicit methods, that overcome this disadvantage, like the Crank-Nicolson Algorithm, which is an unconditionally stable method of solving diffusion-like equations (proof at [7]), which allows for larger steps in the propagation direction.

Extended Crank-Nicolson Algorithm

The algorithm that we used is based on the pages 38-46 from [3]. We want to solve paraxial wave equations of the type:

$$\frac{\partial \mathcal{E}}{\partial z} = \frac{i}{2k_0}\Delta_\perp \mathcal{E} + \mathcal{N}(\mathcal{E}) \qquad (2)$$

where $\mathcal{N}(\mathcal{E})$ represents the medium effects that are to be considered. The code is based on the pseudocode in Table 5, page 45 from [3]. The electric field is represented on a two-dimensional matrix, with longitudinal and radial components. From the Crank-Nicolson recursion equations, we can construct the matrices L_- and L_+ (equations [138],[139] from [3]). The matrices can be adjusted to account for boundary conditions, or change the type of geometry used. Most laser experiments are designed with a cylindrical symmetry, which is why using a cylindrical two-dimensional grid is reasonable for most practical situations. By neglecting the polar angle, we reduce the computational time by a considerable factor. Furthermore, the matrices L_- and L_+ are constructed to have a cylindrical infinitesimal element, which retains the 3D geometry, despite only having two coordinates.

This algorithm is not affected by the grid reflections specific to Fast Fourier transform algorithms,

however, it is affected by boundary reflections. This effect can be diminished by imposing that the last line of L_+ is only composed of zeros. However, by doing this, we do not cancel this effect entirely. In order to do that, we would need to know more about the signal and the channel to be able to construct a perfectly matched layer. Furthermore, even this approach is open to failure, as it is discussed in [6].

If N_r is the dimension of the transverse array, then the dimensions of L_- and L_+ are N_rxN_r. Therefore, the complexity of this approach is similar to the one of the Beam Propagation Method, both in the longitudinal and in the transverse direction. They are also the same in the leaky ($O(n^3)$) and non-leaky ($O(n)$) regime, as leaky signals will also require a greater N_r. However, as we will see, due to the unconditional stability of the algorithm, we can obtain much smaller proportionality constants.

The algorithm works for any smooth function $\mathcal{N}(\mathcal{E})$ which makes the method robust for almost all physical applications. In what follows, we will analyze the output of the code in some known situations, and we will compare it to the known results.

Free space propagation

In this case we took $\mathcal{N}(\mathcal{E}) = 0$ in equation (2). As we can see from Figure 2 (c), we get the expected picture of a diffracting beam. This is best seen when looking at Figure 2 (a), where compare the width of the beam, which is defined by the distance from the center over which the intensity drops by a factor of e, with the analytic expression $w(z) = w_0\sqrt{1 + \left(\frac{z-z_0}{z_r}\right)^2}$. Furthermore, as we can see in Figure 2 (b), the intensity is monotonous, without any unphysical reflections.

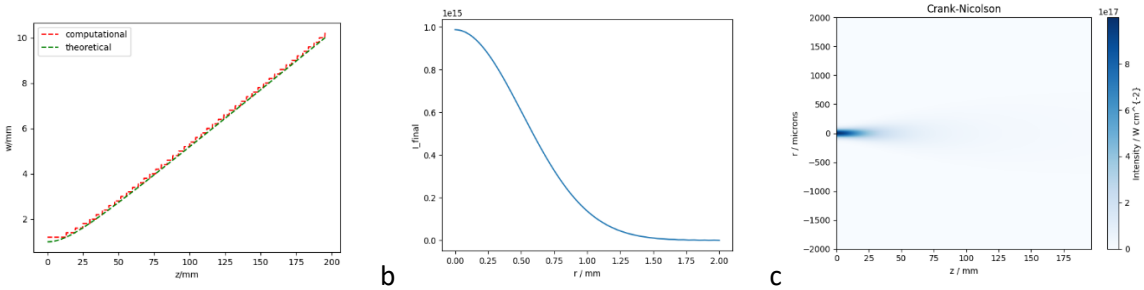

a b c

Figure 2: Propagation of a Gaussian beam of wavelength $\lambda_0 = 800\text{nm}$, intensity $\text{I} = 10^{20}\,\frac{W}{m^2}$ initial spot size $w_0 = 100\mu m$ um over 5 z_R in free space, with the transverse region of interest for the graphs $20\,w_m$, as calculated by a Crank Nicolson code. (a) comparison between the analytic width of the beam and the computational width (b) the transverse intensity profiles of the beam in the exit plane of the channel (c) portrait of the intensity throughout the propagation. For these simulations 50 transverse steps were made, and 20000 longitudinal steps were used.

Parabolic and HOFI channel

For this part, we used the paraxial wave equation for a non-uniform medium, which is derived in [1]:

$$\frac{\partial \mathcal{E}}{\partial \text{z}} = \frac{i}{2k_0}\Delta_\perp \mathcal{E} + \frac{ik_0}{2}(\eta^2 - 1)\mathcal{E} \quad (3)$$

where η is the local index of refraction. For plasma, that is given by $\eta = \sqrt{1 - \frac{e^2 n}{\epsilon_0 m_e \omega^2}}$ (4). By substituting this in the previous equation, we get a formula similar to (2) with $\mathcal{N}(\mathcal{E}) = -\frac{ine^2}{2\epsilon_0 m_e c\omega}\mathcal{E}$. The shape of the beam will be determined by the electron concentration. We know that for a parabolic channel the beam should remain focused (chapter 4 from [2]). For a concentration distribution $\text{n}(r) = \left(n_0 + \frac{\text{r}^2}{w_1^5}\right)$ with $n_0 = 10^{23}, w_1 = 40\mu m$ we obtain the profile in Figure 3 (a), which is what the theory predicts.

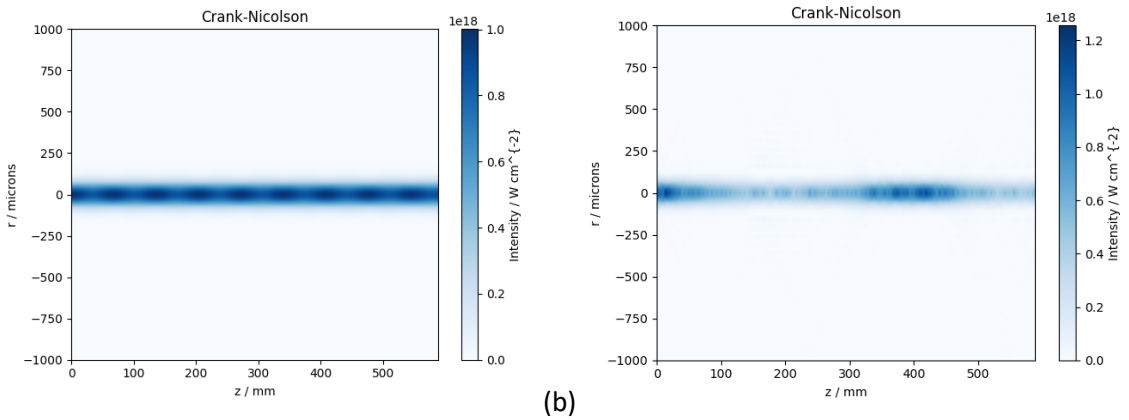

(a) (b)

Figure 3: Propagation of a Gaussian beam of wavelength $\lambda_0 = 800\text{nm}$, intensity $\text{I} = 10^{20}\,\frac{W}{m^2}$ initial spot size $w_0 = 100\mu m$ um over 15 z_R in a channel of matched spot size $w_0 = w_m$, with the transverse region of interest for the graphs $10\,w_m$, as calculated by a Crank Nicolson code (a) in an infinite parabolic channel with $\text{n}(r) = \left(10^{23} + 2.189 * 10^{15}\left(r(nm)\right)^2\right)m^{-3}$ (b) in a HOFI like channel with $n(r) = \left(10^{23} + 2.189 * 10^{15}\left(r(nm)\right)^2\right)m^{-3}, r \leq 150\mu m, n(r) = 0$ otherwise. For these simulations 50 transverse steps were made, and 10000 longitudinal steps were used.

For a HOFI like channel, we assumed the same shape with a linear drop after the cutoff radius r = 50000 nm. As we would expect, the HOFI channel leaks some of the energy, however, even after 15 Rayleigh ranges, most of the energy remains inside the channel.

An extension of these simulations would be taking into consideration the non-linear effects of plasma, such as the Kerr effect described in section 2.4 of [3]. In this case, the medium contribution would be $\mathcal{N}(\mathcal{E}) = -\frac{ine^2}{2\epsilon_0 m_e c\omega}\mathcal{E} + \frac{i\omega_0 n_2 n_0 \epsilon_0 |\mathcal{E}|^2}{2}\mathcal{E}$, with $n_2 = 2\text{x}10^{-19}$ m V^{-2}. As we can, while the 3rd order effects are somewhat neglectable, they tend to help focus the beam through the propagation.

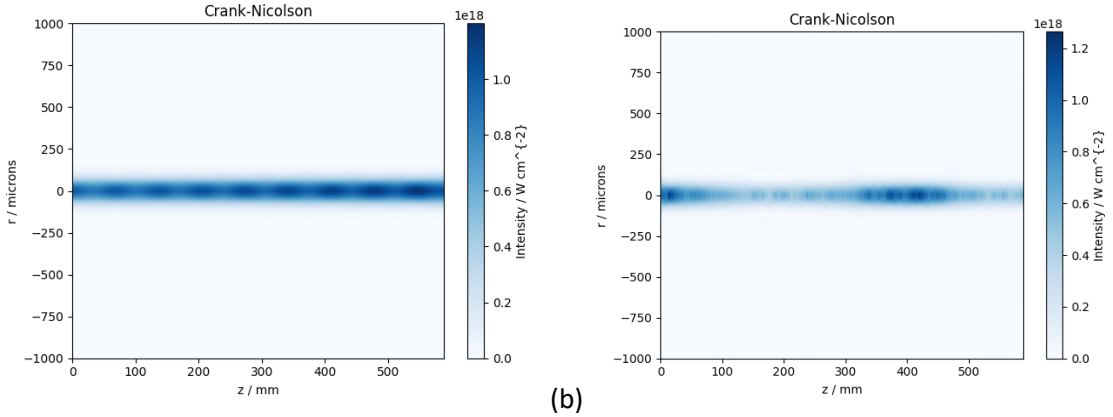

(a) (b)

Figure 4: Propagation similar with the one in Figure 3, but taking into consideration 3rd order effects (a) in an infinite parabolic channel (b) in a HOFI like channel.

<u>Beams with different wavelengths interacting</u>

The code can be used for more than one frequency. In Figure 5 we have a demonstration of how the code works with two different wavelengths in parabolic and HOFI like channels. In both figures, we observe how an interference pattern is formed due to the constructive and destructive interferences of the beams.

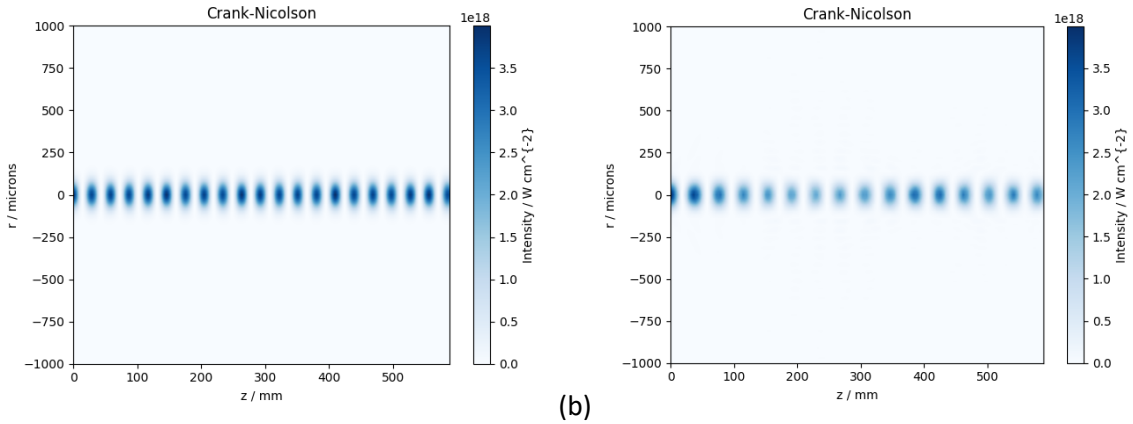

(a) (b)

Figure 5: Propagation of two Gaussian beams of wavelengths (a) $\lambda_0 = 800\text{nm}$ and $\lambda_1 = 400\text{nm}$ (b) $\lambda_0 = 800\text{nm}$ and $\lambda_1 = 500\text{nm}$, intensities $\text{I} = 10^{20}\frac{W}{m^2}$ initial spot sizes $w_0 = 100\mu m$ um over 15 z_R in a channel of matched spot size $w_0 = w_m$, with the transverse region of interest for the graphs $10\,w_m$, as calculated by a Crank Nicolson code(a) in an infinite parabolic channel with $\text{n}(r) = \left(10^{23} + 2.189 * 10^{15}\left(r(nm)\right)^2\right)m^{-3}$ (b) in a HOFI like channel with $n(r) = \left(10^{23} + 2.189 * 10^{15}\left(r(nm)\right)^2\right)m^{-3}, r \leq 150\mu m, n(r) = 0$ otherwise. For these simulations 50 transverse steps were made, and 10000 longitudinal steps were used.

<u>Unmatched spot-size</u>

Another effect that we can test is what happens if the beam width is not similar to the channel width when propagating through a parabolic channel. As we can see, the width of the beam oscillates during the propagation, this dependence is described analytically by formula [96] from [8]: $r_s = \frac{r_i}{2^{0.5}}\sqrt{1 + \frac{n_c r_0^4}{n r_i^4} + \left(1 - \frac{n_c r_0^4}{n r_i^4}\right) cos\left(\frac{2z}{z_R}\sqrt{\frac{n}{n_c}}\right)}$, where n_c is the critical density of plasma and z_R is the Rayleigh range. We can see in Figure 6(c) that the simulation almost perfectly matches the pattern for the fifteen Rayleigh ranges, except for some sharp nonphysical peaks in the last 3 Rayleigh ranges. In Figure 6 (d), we notice that our computation slightly fails to model a wider beam, by obtaining a slightly different oscillation frequency. This might be attributed to the region of interest that is too small.

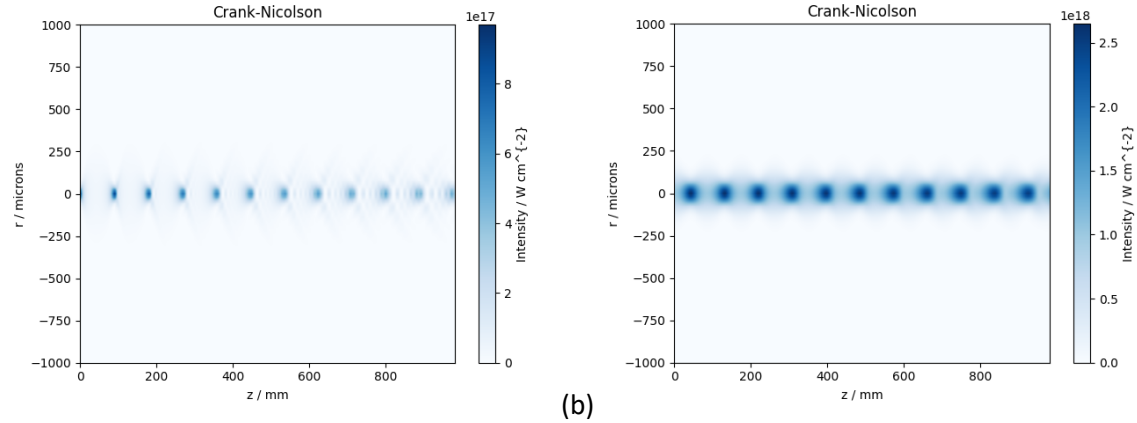

(a) (b)

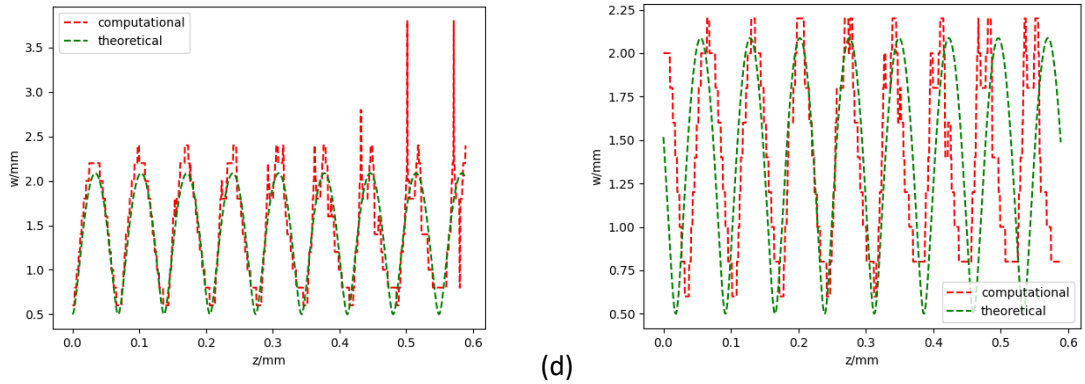

(c) (d)

Figure 6: Propagation over 25 Rayleigh ranges in a parabolic channel with 50 longitudinal steps and 10000 transverse. Comparison of unmatched beam propagation calculated by the Crank-Nicolson code with that predicted by analytical theory. (a, b) the longitudinal variation of the transverse intensity profile I(r) when: (a) $w_0 = \frac{w_m}{2}$; (b) $w_0 = 1.5w_m$. (c, d) Comparison of the longitudinal variation of the beam spot size for: (c) $w_0 = \frac{w_m}{2}$; (d) $w_0 = 1.5w_m$.

Relativistic self-focusing

The self-focusing of laser beams can occur through thermal, relativistic and ponderomotive effects. In this section, we will analyze relativistic self-focusing caused by the mass increase of electrons travelling at speeds approaching the speed of light, which modifies the plasma refractive index of a uniform plasma. Formulas [84-88] from [8] describe this phenomenon. For our laser of wavelength 800nm, the critical power, according to formula [88] from [8] would be P_c = 7.8 GW. We setup a channel with uniform density n = 10^{23} m^{-3}. We change the dependence in formula (2) to accommodate the result in [86]. We are interested in the dependence of the propagation picture with respect to the beam power. For beam powers lower than P_c, we observe that the beam diffracts, which is expected in the non-relativistic regime. However, for powers larger than, the beam starts focusing. As we observe in Figure 7, the beam starts focusing when the power exceeds the critical power. We also notice that is becomes more focused when we increase the power. The profile resembles the one of a parabolic channel, which is expected given that the refractive index profile of accelerated electrons converges to a square dependence.

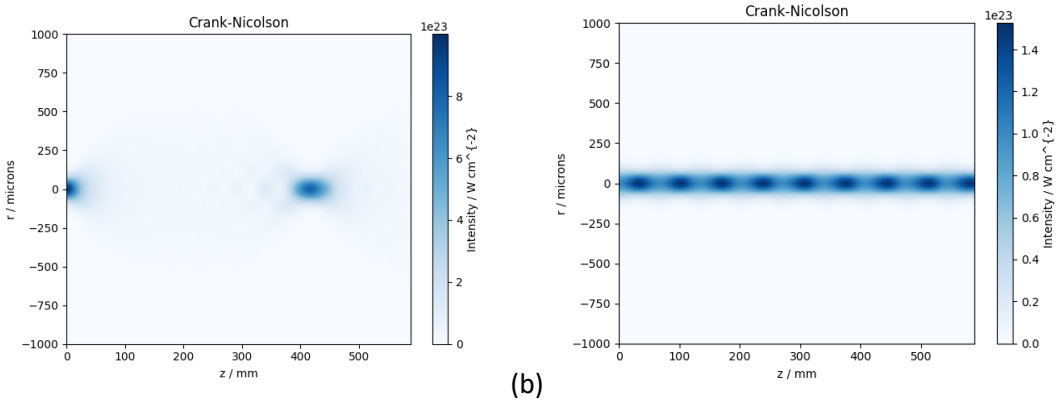

(a) (b)

Figure 7: Propagation of a Gaussian beam of wavelength $\lambda_0 = 800\text{nm}$, power (a) P = 1.05 P_c(b) P = 1.6 Pc, initial spot size $w_0 = 100\mu m$ um over 15 z_R in a medium with uniform density n = 10^{23} m^{-3}, with the transverse region of interest for the graphs 10 w_m, as calculated by a Crank Nicolson code. For these simulations 50 transverse steps were made, and 10000 longitudinal steps were used.

Conclusion

Throughout the situations tested, we noticed that we get physically consistent results when we have 3 or more transverse steps per width of the channel and 200 or more longitudinal steps per Rayleigh range. Taking this into account, the computational constant to propagate one Rayleigh range with a radius of interest of 10 channel widths is of the order of 10^5 which is an order of magnitude lower than the computational constant of the Beam Propagation method, while having the same complexity. Furthermore, the Crank-Nicolson is not subjected to the Fourier-like reflections.

In conclusion, the Crank-Nicolson algorithm is an efficient, robust simulations framework which accurately describes the physical scenario for cylindrically symmetric setups. One improvement that can be added from this point is adding a time dimension, in order to also represent propagations of pulses, rather than just continuous beams.

Acknowledgements

This report is part of the Merton Summer Project Scheme. The project was conducted online for John Adams Institute for Accelerator Science and Department of Physics, University of Oxford, under the supervision of Prof. Simon Hooker.

References

[1] R. Shalloo, Hydrodynamic optical-field-ionized plasma waveguides for laser plasma accelerators, Ph.D. thesis, University of Oxford, Oxford, UK, 2018

[2] B. Miao, Ph.D. Thesis, University of Maryland College Park, 2019

[3] A. Couairon et al., Eur. Phys. J. Special Topics 199, 5–76, 2011

[4] S.M. Hooker, C2 lecture notes: Laser Science and Quantum Information Processing, University of Oxford 2020

[5] A. Picksley, Beam Propagation Code, Department of Physics, University of Oxford, 2020

[6] Ardavan F. Oskooi, Lei Zhang, Yehuda Avniel, Steven G. Johnson, The failure of perfectly matched layers, and towards their redemption by adiabatic absorbers, Optical Society of America, 2008

[7] J. Crank, P. Nicolson, Proc. Camb. Phil. Soc. 43, 50 (1947)

[8] E. Esarey, C. B. Schroeder, and W. P. Leemans, Physics of laser-driven plasma-based electron accelerators, REVIEWS OF MODERN PHYSICS, VOLUME 81, JULY–SEPTEMBER 2009